JOURNAL OF APPLIED PHYSICS VOLUME 90, NUMBER 7 1 OCTOBER 2001

Direct observation of structural changes in organic light emitting devices during degradation

Dmitry Kolosov
Department of Chemistry, University of Southern California, Los Angeles, California 90089

Douglas S. English
Department of Chemistry, University of Texas, Austin, Texas 78712

Vladimir Bulovic
Department of Electrical Engineering, Princeton University, Princeton, New Jersey 08544

Paul F. Barbara
Department of Chemistry, University of Texas, Austin, Texas 78712

Stephen R. Forrest
Department of Electrical Engineering, Princeton University, Princeton, New Jersey 08544

Mark E. Thompson[a)]
Department of Chemistry, University of Southern California, Los Angeles, California 90089

(Received 4 April 2001; accepted for publication 8 June 2001)

A method for studying the degradation of organic light emitting devices (OLEDs) in real time is described. Transparent OLEDs allow for the spatial correlation of cathode topographic images with optical images (transmission, photoluminescence, and electroluminescence) of the devices throughout the degradation process. In this study we focused on the evolution of nonemissive, ''dark'' spots during device operation. We conclude that the electroluminescent dark spots originate as nonconductive regions at the cathode/organic interface and expand or grow as a result of exposure to atmosphere. We propose a mechanism of dark spot growth involving aerobic oxidation of the cathode/organic interfacial region, leading to a highly resistive, carrier blocking interface at the dark spot locations. No initial defects on the cathode surface, which might be responsible for the formation of dark spots, were detected by atomic force microscopy. Structural changes, such as degradation of organic materials and the cathode surface, occur well after the formation and growth of the dark spots. © *2001 American Institute of Physics.* [DOI: 10.1063/1.1389760]

INTRODUCTION

Since the first demonstration of high brightness, low voltage electroluminescence from thin film organic light emitting devices[1] (OLEDs), these structures have attracted considerable interest due to their possible use in a wide range of display applications. There have been many research efforts aimed at understanding the degradation mechanisms of small molecule based OLEDs. The majority of these reliability studies concerned OLEDs employing the common electron transporting material, tris-(8-hydroxyquinoline) aluminum (Alq_3). Two different degradation processes are observed in Alq_3 based devices.[2,3] The first is a long term ''intrinsic'' decay in electroluminescence (EL) intensity leading to a uniform loss of efficiency over the device emitting area. The second process occurs on a somewhat shorter time scale through formation and growth of nonemissive regions or ''dark spots.''[2,4] An inert atmosphere greatly reduces[4] or eliminates[2] the formation and growth of these dark spots. Some reports have tied the formation of cathode ''dome-like textures''[2,5] or ''bubbles''[6,7] to the evolution of dark spots. It has also been proposed that dark spots form as a result of poor carrier injection due to cathode delamination,[2] local degradation of the Alq_3 layer associated with the formation of metal hydroxide sites at the cathode/organic interface,[6] crystallization of either the hole transporting[8] or electron transporting[9] layer, or indium tin oxide (ITO) protrusion sites.[10]

A recent report by Liew *et al.*[11] gives evidence that the dark spot formation in Alq_3-based devices is associated with changes at the cathode/Alq_3 interface. In their study, they operated an OLED until a significant number of dark spots had formed, removed the metal contact, and vacuum deposited a fresh Mg–Ag cathode. This ''rebuilt'' OLED gave uniform emission, with no apparent dark spots. The authors attributed these changes to cathode delamination, however, they did not show direct experimental evidence to support this claim.

Conventional OLEDs utilize a transparent anode and an opaque cathode, the latter typically consisting of a reactive, low work function metal, such as Mg or Ca. The organic layers used in these devices are very thin, ca. 1000 Å, and typically have a large Stokes shift between absorption and emission, making them transparent to their own emission. If the opaque cathode is replaced with a semitransparent Mg–Ag layer capped with an overlayer of ITO, a transparent

[a)]Author to whom correspondence should be addressed; fax: (213) 740-8594; electronic mail: met@usc.edu

 © 2001 American Institute of Physics

Downloaded 13 Dec 2002 to 18.82.1.108. Redistribution subject to AIP license or copyright, see http://ojps.aip.org/japo/japcr.jsp

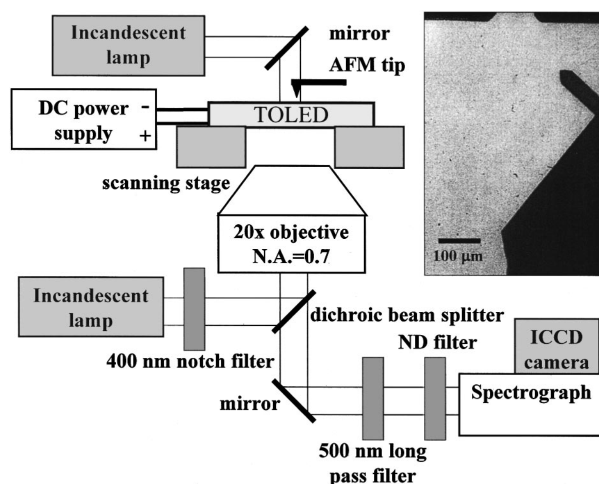

FIG. 1. Experimental setup for measuring EL, PL, TR, and AFM images. The inset shows a transmission image of the device. The AFM tip is clearly seen in the image, allowing the optical and AFM images to be spatially correlated.

OLED, or TOLED, is formed.[12] The transparent cathode has injection and degradation characteristics similar to those of conventional OLEDs (with MgAg, AlLi, or other opaque cathode materials) making TOLEDs good model devices for opaque and transparent OLED degradation studies.[13] The transparency of this device leads to a number of interesting technological applications,[14] as well as making possible the study of OLED degradation. The experiments described here allow for the direct, time resolved, spatial correlation of optical microscopy images [electroluminescence (EL), photoluminescence (PL), and transmission (TR)] with atomic force microscopy (AFM) images of a TOLED obtained throughout the degradation process. Based on our observations we propose a mechanism for the formation and growth of dark spots involving aerobic oxidation reactions.

EXPERIMENT

Transparent organic light emitting devices were fabricated and packaged as previously reported.[12] The 2×2 mm TOLED structure consisted of layers deposited in the following order: ITO/100 Å CuPc/500 Å NPD/500 Å Alq_3/100 Å Mg–Ag (10:1)/400 Å ITO. All layers were deposited by vacuum thermal evaporation at a chamber base pressure of $\times10^{-7}$ Torr, except for the top 400 Å ITO which was sputtered as described elsewhere.[12] A microscope that correlates TR, PL, and EL wide field images with AFM images was used to observe changes in TOLED's physical characteristics as they occurred. A schematic diagram of the experimental setup is given in Fig. 1. The instrument is comprised of a Digital Instruments Bioscope AFM operating in conjunction with a Queensgate NPS100xy closed loop scanning stage mounted on a Zeiss Axiovert inverted fluorescence microscope. The TOLEDs were placed on the sample stage with the Mg–Ag/ITO cathodes facing the AFM tip. Ultrafine adjustment screws were used to precisely position the AFM probe in the region of interest within the optical image field. For these experiments, light emitted from the substrate was collected by a 20× objective (numerical aperture=0.7) and transmitted through a set of neutral density filters to a spectrograph (SP-150, Acton Research Corporation) with an intensified charge coupled detector (ICCD from Princeton Instruments). The spectrograph had a grating and mirror installed on a turret to allow for the acquisition of either the TOLED emission spectra or optical images.

Transmission imaging was achieved by reflecting white light from a fiber bundle off of a 45° mirror mounted above the AFM probe while illuminating the devices from the cathode side. Fluorescence imaging was carried out using epi-illumination with a long-pass dichroic beam splitter. The devices were illuminated at a wavelength of $\lambda=(400\pm10)$ nm from the anode side using filtered light from an incandescent lamp. A $\lambda=500$ nm long pass filter was placed in front of the ICCD to block scattered excitation light. Electroluminescence images were taken when forward bias was applied across the TOLED. (Here forward bias is defined as applying a negative voltage to the cathode as referenced to the anode.) Topographic images of the cathode surfaces were taken with the AFM in the tapping mode using an etched silicon probe. Spatial correlation of the AFM with the optical images is possible because of the device transparency. The AFM tip is clearly visible through the device in the transmission image shown in the inset of Fig. 1.

RESULTS AND DISCUSSION

After TOLED fabrication, the devices were passed from the vacuum system into a nitrogen filled glove box without exposure to the atmosphere. A glass slide was then attached to the substrate with an epoxy seal, encapsulating the TOLED.[4] Electroluminescence (at an applied current of 0.1 mA), PL, and TR images of the packaged devices showed no observable dark spots after several days. The EL and PL spectra of the devices were identical, featuring broad emission with a maximum at $\lambda=530$ nm, typical of Alq_3. The glass slide was removed and the EL image at a current of $I=0.1$ mA was examined briefly in air. Again, no dark spots were observed. A $420\times630\,\mu m^2$ region of the device was then "mapped" by taking nine $90\times90\,\mu m^2$ AFM scans, evenly spaced over the device. Three hours after removing the device encapsulation and mapping the same surface, a constant current of $I=1.5$ mA (40 mA/cm^2) was applied to the TOLED, except for short intervals (2 to 3 min), during which PL and TR images were acquired. During 47 h of running the device, the voltage rose monotonically from 8.5 to 9.8 V.

Electroluminescence images were taken at regular intervals starting 3 h after removing the encapsulation. Images taken at 6, 29, and 44 h are shown in Fig. 2. After the first 4 h of aerobic exposure, very few new dark spots appear. As EL dark spots form and grow, PL and TR images of the device remain uniform and featureless. It is not possible to differentiate the EL emissive and nonemissive areas of the TOLED in the PL and TR images. Under constant total current injection, the light intensity of the emissive areas monotonically increases as the EL dark spots grow, supporting the suggestion made by McElvain *et al.*[2] that the dark spots are regions of low conductivity. As observed previously by Bur-

Downloaded 13 Dec 2002 to 18.82.1.108. Redistribution subject to AIP license or copyright, see http://ojps.aip.org/japo/japcr.jsp

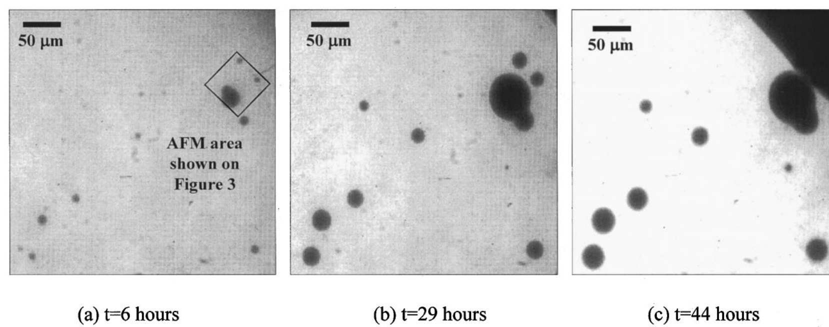

FIG. 2. EL images reflecting evolution of dark spot growth in the TOLED. The device was exposed to the air for 3 h and then run at a constant current of 1.5 mA ($40\,\mathrm{mA/cm^2}$). Times quoted as the total time in the air. (a) $t=6$ h, (b) $t=29$ h, and (c) $t=44$ h.

rows *et al.*,[4] a dark front moves in from the contact edges, gradually consuming the EL active regions of the device. This front can be seen in Figs.2(b) and 2(c), advancing from the upper right-hand corner. The advance of this front is considerably faster than the rate of the dark spot growth.

Evolution of the cathode morphology was monitored using AFM (Fig. 3) in the region corresponding to the box in Fig. 2(a). The image in Fig. 3(a) was recorded 1 h after the package cover had been removed (before the constant current was applied), and shows no surface features. The rms roughness of the film is 3 nm, similar to ITO coated glass substrates. After running the device at $I=1.5\,\mathrm{mA}$ for 3 h (6 h total in air), three dark spots appear in the region of the device shown in the EL image, Fig. 3(b). The EL and AFM images are taken on opposite sides of the TOLED, so they have a mirror relationship to each other and hence the image in Fig. 3(b) is reversed to simplify its comparison to the AFM images. Comparing Figs. 3(a) and 3(b), there are no identifiable defects in the AFM scans where the dark spots are present. This observation is contrary to previous reports which have suggested that dark spots are the result of defects in the cathode, or are due to large particles present on the substrate prior to organic and metal film deposition.[2,4,7,9,10] Delamination has also been proposed as a mechanism for dark spot formation and growth,[2,7] although, once again we find no evidence for this in our experiments. The AFM scan over the area of dark spots, shown in Fig. 3(c), shows no topographical differences between the dark spots and the

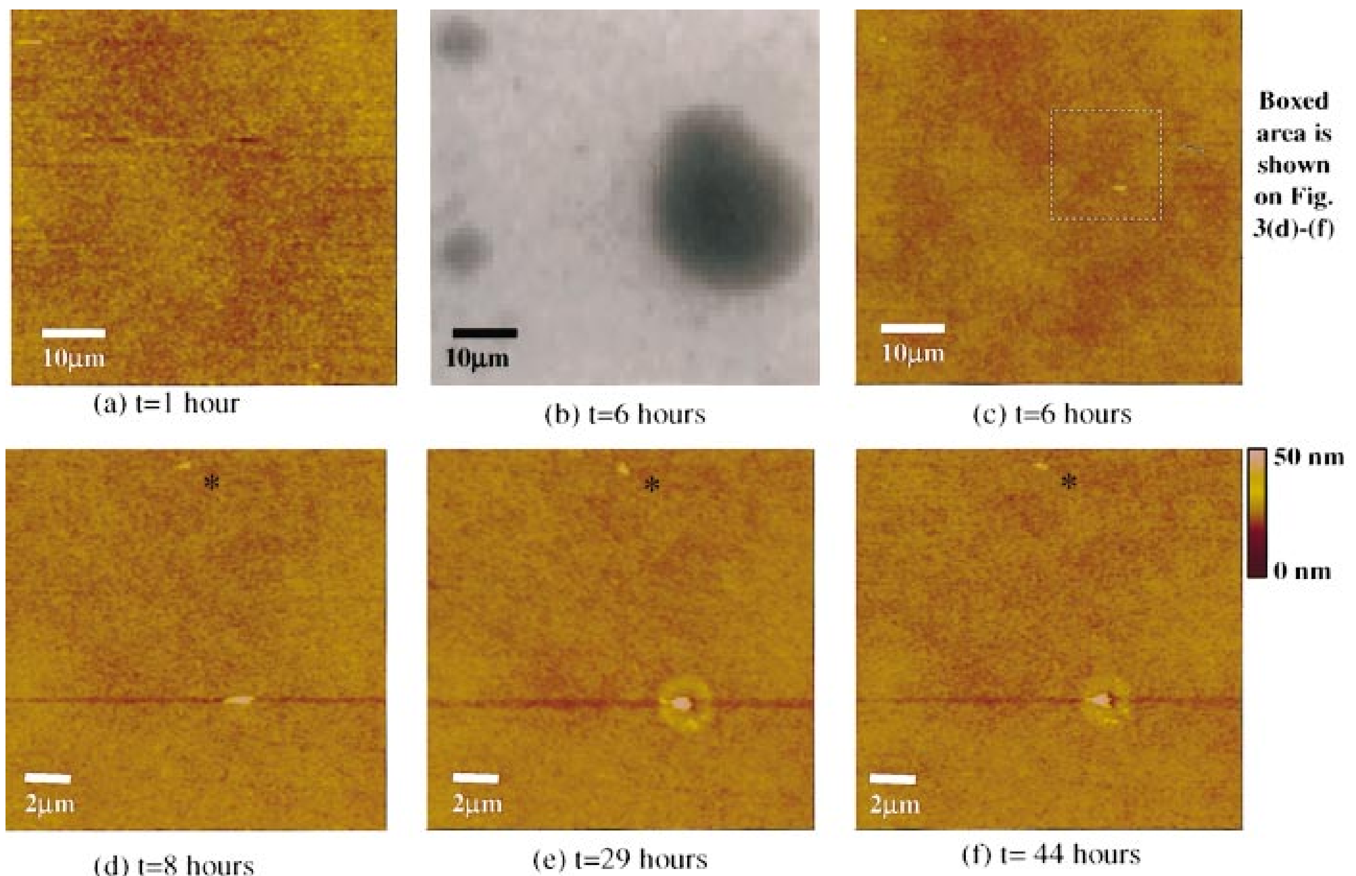

FIG. 3. (Color) Spatially correlated AFM and EL images of the TOLED used for Fig. 2. (a) AFM scan taken 1 h after removing the device encapsulation and before applying bias to the device. (b) EL image spatially correlated to the cathode area [designated by the box in Fig. 2(a)], $t=6$ h, (c) An AFM scan of the same area, $t=6$ h. AFM scans of the area designated by the box in (c) are shown at $t=8$ h (d), at $t=29$ h (e), and at 44 h (f).

Downloaded 13 Dec 2002 to 18.82.1.108. Redistribution subject to AIP license or copyright, see http://ojps.aip.org/japo/japcr.jsp

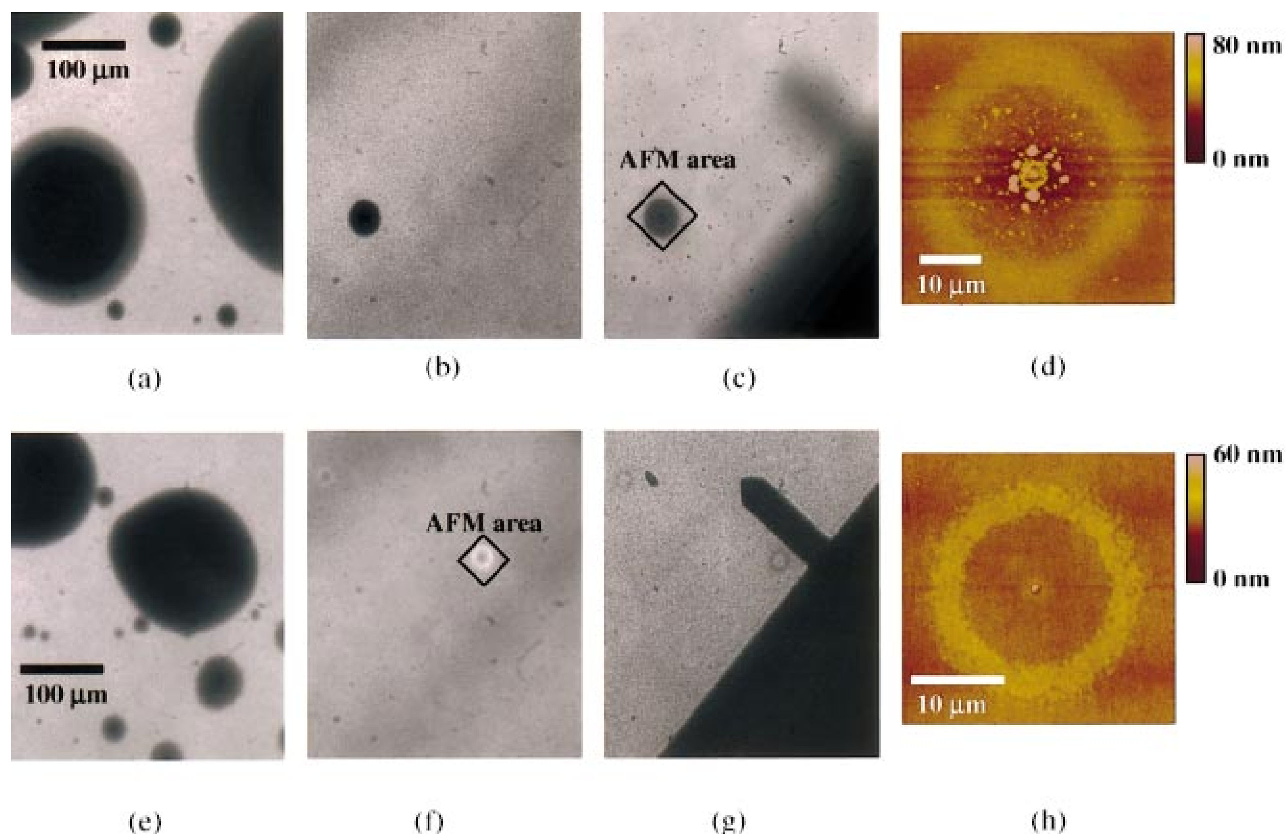

FIG. 4. (Color) Time and spatially correlated images of two TOLEDs, which spent 92 h in room ambient. Device 1 was run for 61 h at constant current of 1.5 mA, no bias was applied to device 2. Images of device 1 are shown in (a) EL, (b) PL, (c) TR, and (d) AFM image of the area designated at (c). Images of device 2 are shown in (e) EL, (f) PL, (g) TR, and (h) AFM image of the area designated at (f).

bright areas surrounding them. Further, there are no topographical features at the edges of the dark spot, and no detectable height differences between the EL emissive and dark spot regions of the device. While our AFM data do not exclude the possibility of a slight delamination (0.5–1 nm) of the cathode and Alq_3 layers, the formation of more pronounced bubbles[6,7] or dome-like structures[2,5] is clearly not observed.

In the early stages of device degradation, small features are often observed near the centers of the dark spots, however, they are not always present in subsequent AFM scans. It is not possible to determine with certainty if these are real topographic features or artifacts of the AFM imaging process. Artifacts could result from AFM tip charging, leading to repulsive interactions between the tip and cathode of the electrically biased device; intermittent artifacts could result from a fouled AFM tip depositing material in these areas of the device, or other processes that are unrelated to physical changes in cathode morphology.

As the device ages further, a permanent feature near the center of the dark spot appears and grows, ultimately forming a raised region immediately around a tall protrusion [Figs. 3(d)–3(f)].[15] The raised region may result from delamination, although the region is significantly smaller than the dark spot.

After studying the TOLEDs for 4 days, their optical and AFM images were compared to devices having spent the same amount of time in the air (adjacent TOLEDs on the same substrate), but with no bias applied. Electroluminescence images of the unstressed devices show densities and sizes of dark spots similar to TOLEDs that had been under nearly continuous operation. Figures 4(a)–4(d) show images of a device that was operated for 61 h at 1.5 mA (92 h total in the air). Figures 4(e)–4(h) are images of a device which spent the same amount of time in the air, but with no bias applied. In contrast to the TOLEDs in early stages of degradation, the large EL dark spots of the stressed device have correlated circular dark spots in both the PL and TR images. The PL and TR dark spots have the same center locations as the corresponding EL dark spots, but are significantly smaller in size. The AFM image of the dark spots revealed that these regions contained a raised, ring-shaped structure, with additional large features inside the ring, Fig. 4(d). The optical and topographic images show that the cathode and the underlying Alq_3 are damaged in the later stages of device degradation.

Large EL dark spots of the unstressed device have correlated features on the PL and TR images as well, seen as bright and dark rings, respectively, in Figs. 4(f) and 4(g). The AFM image of the unstressed device in Fig. 4(h) shows a raised ring, very similar to the one seen in the stressed device, which is the same size as the correlated PL and TR features in Figs. 4(f) and 4(g) of the unstressed TOLED. In contrast to the stressed device, however, the raised ring in Fig. 4(h) has only a single particle located at its center. These rings may designate cathode areas which have delaminated from the emitting Alq_3 layer. Enhanced PL is expected for a

Downloaded 13 Dec 2002 to 18.82.1.108. Redistribution subject to AIP license or copyright, see http://ojps.aip.org/japo/japcr.jsp

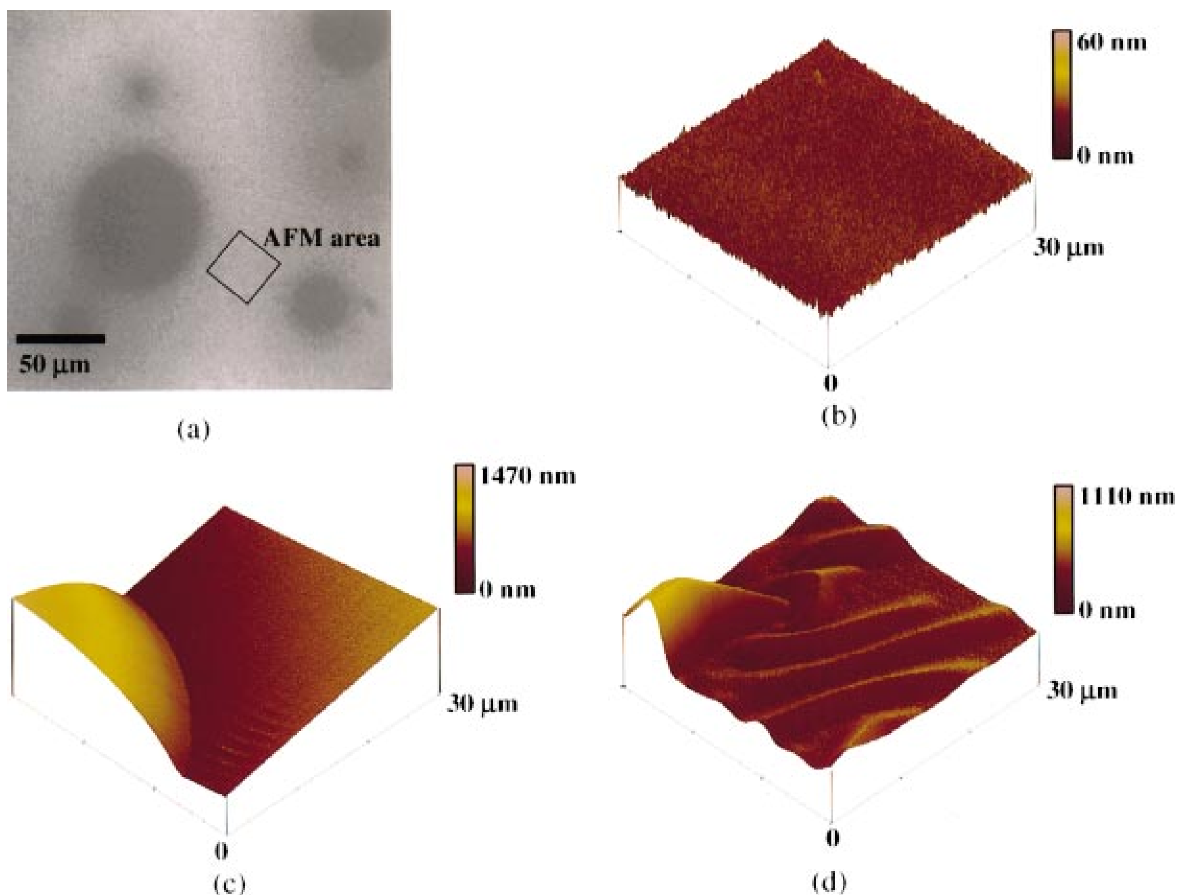

FIG. 5. (Color) Electroluminescence image showing the AFM area (a) as well as the AFM images of the device at time $t=0$, applied voltage 11 V (b), at time $t=160$ min, applied voltage 14 V (c), and of the fully degraded device (d). The bubble seen in (c) was formed shortly after the bias was increased to 14 V.

delaminated cathode since exciton quenching at the free surface of Alq_3 is reduced.

Dome-like structures[2,5] or bubbles[6,7] were not observed during our degradation studies. To investigate whether the previously reported bubble-like features were related to stress caused by operating the device, we examined devices operated at markedly higher power levels. AFM scans were taken in the area between two dark spots as shown in Fig. 5(a). The AFM image in Fig. 5(b) was taken at the beginning of the experiment with an applied bias of 11 V ($J=100\,\mathrm{mA/cm^2}$), which is significantly higher than the bias used in the experiments described above (8.5–9.8 V, $J=40\,\mathrm{mA/cm^2}$). There were no detectable changes in cathode morphology for 2 h at the higher bias conditions. When the bias was increased to 14 V ($J=250\,\mathrm{mA/cm^2}$), the cathode surface morphology changed abruptly. Initially the surface exhibited large (several μm high) and rapidly changing features. Thirty minutes later, a large bubble (height $\sim 1.5\,\mu$m) was observed [Fig. 5(c)] to stabilize under constant bias. AFM images of the top and adjacent to the bubble appear nearly featureless with no signs of rupture of the cathode surface. The AFM image in Fig. 5(d) was taken after the EL emission from this area of the device had completely ceased as a result of a further increase in bias (to 16 V). The resulting surface appeared rippled and irregular, with vertical features of ~ 1000 nm. Cathode bubbles have been previously attributed to gas evolution processes.[5,7] This is consistent with our studies which show that bubble formation is related to the power applied to the device (and hence heat generated), and can form in regions free from obvious defects on the surface.

MECHANISTIC DISCUSSION

It has been proposed that oxidation occurs in EL dark spot regions and leads to the formation of a metal hydroxide at the cathode/organic ingterface.[6] Based on our observations we propose a related, oxidation-based mechanism for dark spot formation and growth. Water and oxygen from the air may diffuse into the device through microscopic pinholes, cracks, or grain boundaries in the cathode which are too small to be detected by AFM. Oxygen and water enter through these defects and lead to oxidation reactions at the Mg/organic interface, forming an insulating layer. The oxidation reaction could involve the magnesium electrode itself, leading to electrically insulating magnesium oxide or hydroxide at the interface between the cathode and organic film, creating a barrier to electron injection. An alternate oxidation process that may be prevalent at the early stages of dark spot formation and growth involves reduced Alq_3 molecules (Alq_3^-), formed near the cathode/Alq_3 interface during thermal deposition of Mg.[16] The reduced Alq_3 facilitates electron injection into the layer bulk. Oxidation of surface Alq_3^- would lead to poor electron injection, forming EL

Downloaded 13 Dec 2002 to 18.82.1.108. Redistribution subject to AIP license or copyright, see http://ojps.aip.org/japo/japcr.jsp

dark spots. Interfacial Alq_3^- oxidation is not expected to lead to a significant change in film thickness in the dark spots since only a small fraction of the layer is reduced on thermal deposition of Mg.

After extended exposure to the air, bulk cathode oxidation may occur, leading to a measurable increase in device thickness. But the dark spots should grow faster and larger than the raised regions in the AFM images, as observed. Diffusion of oxygen and moisture from the edges of the device occurs faster than at dark spots since the surface area is significantly larger at the edge than at the microscopic cathode defects. This leads to a more rapid growth of the dark fronts than dark spots. Since the process proposed for formation and growth of dark spots involves aerobic oxidation, the dark spot growth is expected to occur at similar rates in unstressed devices stored in the air, as well as devices being driven in the air.

Aziz *et al.* reported[9] that exposure to humidity induces the formation of Alq_3 crystallites in originally amorphous films. Those crystals form protruding lumps that are several times thicker than the original film, and have a water content higher than that in the amorphous Alq_3 regions. The diffusion of water into the device through microscopic defects in the cathode may lead to crystallization of Alq_3 in the OLED structure itself, leading to growth of Alq_3 crystals. These crystals enlarge the defects in the cathode and ultimately appear on the cathode surface as large grains, e.g., Figs. 3(d) and 3(e). The Alq_3 grains formed in the early stages of device degradation may be small and easily swept away by the AFM tip, possibly explaining the intermittent features observed in the AFM images in the first 10–15 h of device degradation.

CONCLUSIONS

We have found that EL dark spots in OLEDs originate as nonconductive areas at the metal/organic interface, and rapidly grow as a result of atmospheric exposure. The dark spots are attributed to regions of poor electron injection formed by local oxidation. Continuous diffusion of oxygen and water into the device leads to growth of the oxidized region of the cathode, radially from the central defect. Significant structural changes in the cathodes occur well after the initial formation and growth of the EL dark spots take place. In contrast to the growth of dark spots, bubble formation was found to be enhanced at high current densities.

While crystallite growth in the Alq_3 contributes to the cathode morphological changes observed, the principal causes of dark spot formation and growth are oxidation reactions at the cathode/electron-transporting-layer interface. This oxidation could involve the cathode itself, leading to a resistive oxide layer between the cathode and the Alq_3, or it could involve a reduced region within the bulk transport layer. A reduced interfacial region (forming midgap states) near the cathode is critical to achieving a low barrier to electron injection, even for cathode materials that are air stable (e.g., ITO[17] or Ag[18]). As a result, dark spot formation and growth may still occur due to oxidation of the reduced Alq_3 in the cathode/organic interfacial region.

ACKNOWLEDGMENTS

The authors thank Universal Display Corporation, the Defense Advanced Research Projects Agency, and the National Science Foundation for financial support of this work.

[1] C. W. Tang and S. A. VanSlyke, Appl. Phys. Lett. **51**, 913 (1987).
[2] J. McElvain, H. Antoniads, M. R. Hueschen, J. N. Miller, D. M. Roitman, J. R. Sheats, and R. L. Moon, J. Appl. Phys. **80**, 6002 (1996).
[3] H. Aziz, Z. D. Popovic, N. X. Hu, A. M. Hor, and G. Xu, Science **283**, 1900 (1999); Z. D. Popovic, H. Aziz, N. Hu, A. Hor, and G. Xu, Synth. Met. **111–112**, 229 (2000).
[4] P. E. Burrows, V. Bulovic, S. R. Forrest, L. S. Sapochak, D. M. McCarty, and M. E. Thompson, Appl. Phys. Lett. **65**, 2922 (1994).
[5] L. M. Do, M. Oymada, A. Koike, E. Han, N. Yamamoto, and M. Fujihira, Thin Solid Films **273**, 209 (1996).
[6] H. Aziz, Z. Popovic, C. P. Tripp, N. X. Hu, A. M. Hor, and G. Xu, Appl. Phys. Lett. **72**, 2642 (1998).
[7] L. S. Liao, J. He, X. Zhou, Z. H. Xiong, Z. B. Deng, X. Y. Hou, and S. T. Lee, J. Appl. Phys. **88**, 2386 (2000).
[8] P. F. Smith, P. Gerroir, S. Xie, A. M. Hor, Z. Popovic, and M. L. Hair, Langmuir **14**, 5964 (1998).
[9] H. Aziz, Z. Popovic, S. Xie, A. M. Hor, N. X. Hu, C. Tripp, and G. Xu, Appl. Phys. Lett. **72**, 756 (1998).
[10] M. Kawaharada, M. Ooishi, T. Saito, and E. Hasegawa, Synth. Met. **91**, 113 (1997).
[11] Y. F. Liew, H. Aziz, N. X. Hu, H. S. Chan, G. Xu, and Z. Popovic, Appl. Phys. Lett. **77**, 2650 (2000).
[12] V. Bulovic, G. Gu, P. E. Burrows, M. E. Thompson, and S. R. Forrest, Nature (London) **380**, 29 (1996); G. Gu, V. Bulovic, P. E. Burrows, S. R. Forrest, and M. E. Thompson, Appl. Phys. Lett. **68**, 2606 (1996).
[13] P. E. Burrows, G. Gu, S. R. Forrest, E. P. Vicenzi, and T. X. Zhou, J. Appl. Phys. **87**, 3080 (2000).
[14] P. E. Burrows, G. Gu, V. Bulovic, Z. Shen, S. R. Forrest, and M. E. Thompson, IEEE Trans. Electron Devices **44**, 1188 (1997); G. Gu, G. Parthasarathy, P. Tian, P. E. Burrows, and S. R. Forrest, J. Appl. Phys. **86**, 4076 (1999).
[15] A small feature is seen in these higher resolution AFM images [Figs. 3 (d)–(f)], labeled with an asterisk. This feature does not change in size or shape over time and is most likely a dust particle or other foreign object. This particle and its spatial relationship to the evolving feature in the center of the image were used to maintain the spatial correlation of the AFM images over time.
[16] L. S. Hung, C. W. Tang, and M. G. Mason, Appl. Phys. Lett. **70**, 152 (1997); J. Kido and T. Matsumoto, *ibid.* **73**, 2866 (1998); L. S. Hung and C. W. Tang, *ibid.* **74**, 3209 (1999); H. Ishi, K. Sugiyama, E. Ito, and K. Seki, Adv. Mater. **11**, 605 (1999); E. I. Haskal, A. Urioni, P. F. Seidler, and W. Androni, Appl. Phys. Lett. **71**, 1151 (1997); R. Schlaf, B. A. Parkinson, P. A. Lee, K. W. Nebesny, and N. R. Armstrong, *ibid.* **73**, 1026 (1998).
[17] G. Gu, G. Parthasarathy, and S. R. Forrest, Appl. Phys. Lett. **74**, 305 (1999).
[18] Y. Sato, T. Ogata, S. Ichinosawa, M. Fugono, and H. Kanai, Proc. SPIE **3797**, 198 (1999); H. Kanai, S. Ichinosawa, and Y. Sato, Synth. Met. **91**, 195 (1997).

Downloaded 13 Dec 2002 to 18.82.1.108. Redistribution subject to AIP license or copyright, see http://ojps.aip.org/japo/japcr.jsp